Hydrol. Earth Syst. Sci. Discuss., 11, 7053–7087, 2014
www.hydrol-earth-syst-sci-discuss.net/11/7053/2014/
doi:10.5194/hessd-11-7053-2014

Hydrology and Earth System Sciences
Open Access
Discussions

Analytical approach for predicting fresh water discharge in an estuary based on tidal water level observations

H. Cai[1], **H. H. G. Savenije**[1], **and C. Jiang**[2]

[1]Department of Water Management, Faculty of Civil Engineering and Geosciences, Delft University of Technology, Stevinweg 1, P.O. Box 5048, 2600 GA Delft, the Netherlands
[2]School of Hydraulic, Energy and Power Engineering, Yangzhou University, Yangzhou 225127, China

Received: 22 May 2014 – Accepted: 10 June 2014 – Published: 27 June 2014

Correspondence to: H. Cai (h.cai@tudelft.nl)

Published by Copernicus Publications on behalf of the European Geosciences Union.

Abstract

As the tidal wave propagates into an estuary, the tidally averaged water level tends to rise in landward direction due to the density difference between saline and fresh water and the asymmetry of the friction. The effect of friction on the residual slope is even more remarkable when accounting for fresh water discharge. In this study, we investigate the influence of river discharge on tidal wave propagation in the Yangtze estuary with specific attention to residual water level slope. This is done by using a one-dimensional analytical model for tidal hydrodynamics accounting for the residual water level. We demonstrate the importance of the residual slope on tidal dynamics and use it to improve the prediction of the tidal propagation in estuaries (i.e., tidal damping, velocity amplitude, wave celerity and phase lag), especially when the influence of river discharge is significant. Finally, we develop a new inverse analytical approach for estimating fresh water discharge on the basis of tidal water level observations along the estuary, which can be used as a tool to obtain information on the river discharge that is otherwise difficult to measure in the tidal region.

1 Introduction

Estuaries are water bodies that form the transition between an ocean (or sea) and a river. Their specific hydraulic behaviour is unique in that they are not merely a mixture of marine and a riverine signatures, experiencing both the effect of tides and of river discharge, but that they have a very specific hydraulic behaviour with a phase lag somewhere between that of a progressive and standing wave, a strongly deformed tidal wave and a residual water level slope due to the presence of a density gradient and the asymmetry of the friction between ebb and flood currents (e.g. Savenije, 2012). This asymmetry is even strengthed by river discharge. Due to the inherent funnel shape of estuaries, the effect of river discharge is much smaller near the estuary mouth, where the cross-sectional area is generally orders of magnitude larger than the cross-section

HESSD
11, 7053–7087, 2014

of the river, but it can become dominant further upstream in the estuary, particularly during times when the river is in spate.

Due to the general dominance of tidal flows in the tidal region of an estuary, it is often difficult to determine the magnitude of the fresh water discharge accurately in estuaries. Knowing the fresh water discharge within the tidal region, however, may be important for the purpose of irrigation or for estimating the effect of water withdrawals on salt intrusion (e.g. Zhang et al., 2012a). Several methods have been presented to estimate the fresh water discharge in estuaries (e.g. Miller et al., 2006; Negrel et al., 2011; Moftakhari et al., 2013; Hidayat et al., 2014). However, most of them are statistical analyses without using an analytical relationship between the fresh water discharge and other controlling parameters (such as water level and tidal damping). In this paper, we establish an analytical equation relating tidal wave propagation to the fresh water discharge from upstream. Besides the general interest of establishing an analytical relation between wave cererity, phase lag, velocity amplitude, tidal damping, residual slope and river discharge, this relationship can be of practical use to estimate, in an inverse way, river discharge on the basis of observed tidal water levels along the estuary axis.

The Yangtze estuary in China is used as an illustration of the analytical approach. The tidal dynamics of the Yangtze estuary was earlier investigated by Zhang et al. (2012.) using an analytical model proposed by Savenije et al. (2008). They calibrated their model on data observed during the dry season assuming that the effect of river discharge was negligible. In this paper, we elaborate on the analytical solutions proposed by Cai et al. (2014) and investigate the influence of residual water level on tidal dynamics, which is poorly known, especially during the wet season when there is strong river discharge. In the method section, we build on the analytical approach proposed by Cai et al. (2014) accounting for the effect of river discharge. The method consists of two parts. The first part still considers a fixed tidally averaged depth, while the second part involves an iterative procedure to account for the residual water level slope due to nonlinear friction. In Sect. 3, the analytical model is applied to the Yangtze estuary and

HESSD
11, 7053–7087, 2014

the way how river discharge affects the tidal damping is discussed. Subsequenly, we propose a new method to estimate fresh water discharge based on observed tidal water levels in the upstream part of an estuary. Finally, conclusions are drawn in Sect. 4.

2 Method

2.1 Analytical model for tidal dynamics accounting for river discharge

The basic geometric assumption of the analytical model is that the shape of alluvial estuaries can be descried by exponential functions of tidally average cross-sectional area, width, and depth (e.g. Savenije, 2005, 2012):

$$\overline{A} = \overline{A_0}\exp\left(-\frac{x}{a}\right), \qquad \overline{B} = \overline{B_0}\exp\left(-\frac{x}{b}\right), \qquad \overline{h} = \overline{h_0}\exp\left(-\frac{x}{d}\right), \tag{1}$$

where x is the longitudinal coordinate directed landward, $\overline{A}$, $\overline{B}$, $\overline{h}$ are the tidally averaged cross-sectional area, stream width, and flow depth, a, b, d are the convergence lengths of the cross-sectional area, width, and depth, respectively, and the subscript 0 relates to the reference point near the estuary mouth.

A second assumption is that the flow width may be assumed to be constant in time while the lateral storage variation is described by the storage width ratio $r_S = \overline{B}/B_S$ where B_S is the storage width (Savenije et al., 2008). Finally, the instantaneous flow velocity V of a moving particle is considered to consist of a steady component U_r, caused by the fresh water discharge, and a time-dependent component U_t, contributed by the tide:

$$V = U_t - U_r, \qquad U_t = \upsilon\sin(\omega t), \qquad U_r = Q_f/\overline{A}, \tag{2}$$

where t is time, Q_f is the river discharge, υ is the tidal velocity amplitude, and ω is the tidal frequency.

HESSD
11, 7053–7087, 2014

It has been shown that the estuarine hydrodynamics of an arbitrary cross-section is controlled by a four dimensionless parameters that depend only on the local (i.e., fixed position) geometry and on the external forcing (Toffolon et al., 2006; Savenije et al., 2008; Toffolon and Savenije, 2011; Cai et al., 2012, 2014). Table 1 presents these dimensionless parameters, including: ζ the dimensionless tidal amplitude, γ the estuary shape number, χ the friction number, and φ the dimensionless river discharge, where η is the tidal amplitude, c_0 is the classical wave celerity of a frictionless progressive wave in a constant-width channel:

$$c_0 = \sqrt{g\bar{h}/r_S}, \tag{3}$$

and f is the dimensionless friction factor resulting from the envelope method (Savenije, 1998), defined as:

$$f = \frac{g}{K^2\bar{h}^{1/3}}\left[1 - \left(\frac{4}{3}\zeta\right)^2\right]^{-1}, \tag{4}$$

where K is the Manning–Strickler friction coefficient, the factor 4/3 stems from a Taylor approximation of the exponent of the hydraulic radius in the friction term (it implies that ζ should be smaller than 3/4).

The dependent dimensionless variables are also shown in Table 1, where δ is the damping number (a dimensionless description of the increase, $\delta > 0$, or decrease, $\delta < 0$, of the tidal wave amplitude along the estuary), μ the velocity number (the actual velocity amplitude scaled by the frictionless value in a prismatic channel), λ the celerity number (the ratio between the theoretical frictionless celerity in a prismatic channel c_0 and the actual wave celerity c) and ε the phase lag between high water (HW) and high water slack (HWS) or between low water (LW) and low water slack (LWS). For a simple harmonic wave $\varepsilon = \pi - (\phi_Z - \phi_U)$, where ϕ_Z and ϕ_U are the phase of water level and velocity, respectively (Toffolon et al., 2006; Savenije et al., 2008).

HESSD
11, 7053–7087, 2014

Making use of the dimensionless parameters presented in Table 1, Cai et al. (2014) demonstrated that the analytical solutions for tidal dynamics in a local cross-section can be obtained by solving a set of 4 equations (see Table 2), i.e., the phase lag Eq. (T1), the scaling Eq. (T2), the celerity Eq. (T3), and the damping Eq. (T4), where

$$\beta = \theta - r_S \zeta \frac{\varphi}{\mu\lambda}, \qquad \theta = 1 - \left(\sqrt{1+\zeta} - 1\right)\frac{\varphi}{\mu\lambda}, \tag{5}$$

and Γ_H is a hybrid friction term that is obtained by a combination of the linearized and the nonlinear Lagrangean friction term, with the optimum weight of the linearized friction term Γ_L being 1/3, and 2/3 of the nonlinear friction term Γ:

$$\Gamma_H = \frac{2}{3}\Gamma + \frac{1}{3}\Gamma_L, \tag{6}$$

with

$$\Gamma = \begin{cases} \mu\lambda\left[1 + \frac{8}{3}\zeta\frac{\varphi}{\mu\lambda} + \left(\frac{\varphi}{\mu\lambda}\right)^2\right] & \text{for } \varphi < \mu\lambda \\ \mu\lambda\left[\frac{4}{3}\zeta + 2\frac{\varphi}{\mu\lambda} + \frac{4}{3}\zeta\left(\frac{\varphi}{\mu\lambda}\right)^2\right] & \text{for } \varphi \geq \mu\lambda \end{cases} \tag{7}$$

$$\Gamma_L = \frac{L_1}{2} - \zeta\frac{L_0}{3\mu\lambda}, \tag{8}$$

If $\varphi < 1$, the expressions of coefficients L_0 and L_1 are given by (Dronkers, 1964, P272–275):

$$L_0 = [2 + \cos(2\alpha)]\left(2 - \frac{4\alpha}{\pi}\right) + \frac{6}{\pi}\sin(2\alpha), \tag{9}$$

$$L_1 = \frac{6}{\pi}\sin(\alpha) + \frac{2}{3\pi}\sin(3\alpha) + \left(4 - \frac{8\alpha}{\pi}\right)\cos(\alpha), \tag{10}$$

HESSD
11, 7053–7087, 2014

with

$$\alpha = \arccos(-\varphi)\,. \tag{11}$$

If $\varphi \geq 1$, these coefficients become:

$$L_0 = -2 - 4\varphi^2\,, \qquad L_1 = 4\varphi\,, \tag{12}$$

If the river discharge is negligible ($U_r = 0$), the damping Eq. (T4) (see Table 2) can be simplified as:

$$\delta = \frac{\mu^2}{1+\mu^2}\left(\gamma - \chi\mu\lambda\Gamma_H\right), \tag{13}$$

with

$$\Gamma_H = \frac{2}{3}\mu\lambda + \frac{8}{9\pi}\,, \tag{14}$$

which corresponds to Eq. (27) of Cai et al. (2012).

As an illustration, Fig. 1 shows the variation of the main dependent dimensionless parameters as a function of the shape number γ and the dimensionless river discharge φ for given values of $\zeta = 0.1$, $\chi = 2$ and $r_S = 1$, where the red lines represent the values in an ideal estuary (with no damping or amplification, i.e., $\delta = 0$, $\lambda = 1$), of which the solutions are also presented in Table 2.

HESSD
11, 7053–7087, 2014

2.2 Iterative proceduce to account for the residual water level

Building on the work by Vignoli et al. (2003), Cai et al. (2014)proposed an analytical formula to calculate the residual water level:

$$\overline{z}(x) = -\int_0^x \frac{\overline{V|V|}}{K^2 h^{4/3}} \mathrm{d}x\,, \qquad \frac{\overline{V|V|}}{K^2 h^{4/3}} \approx \frac{1}{2}\left[\frac{V_{\mathrm{HW}}|V_{\mathrm{HW}}|}{K^2\left(\overline{h}+\eta\right)^{4/3}} + \frac{V_{\mathrm{LW}}|V_{\mathrm{LW}}|}{K^2\left(\overline{h}-\eta\right)^{4/3}}\right], \tag{15}$$

where V_{HW} and V_{LW} are the instantaneous velocities at HW and LW:

$$V_{\mathrm{HW}} = \upsilon\sin(\varepsilon) - U_{\mathrm{r}}\,, \qquad V_{\mathrm{LW}} = -\upsilon\sin(\varepsilon) - U_{\mathrm{r}}\,. \tag{16}$$

It is important to recognize that Eq. (15) does not account for the effect of density difference between ocean and river water, which results in a residual water level slope amounting to 1.25 % of the estuary depth over the salt intrusion length (see Savenije, 2005, P37). Since the resulted residual water level is relatively small compared with the tidally averaged depth and it is concentrated in the seaward part of an estuary, we neglect the density effect in this paper. Consequently, the tidally averaged depth including the residual water level is:

$$\overline{h_{\mathrm{new}}}(x) = \overline{h}(x) + \overline{z}(x)\,. \tag{17}$$

where $\overline{h}$ is the depth in relation to mean sea level.

The generic water levels in a tidal channel is illustrated in Fig. 2. For the case of negligible river discharge ($U_{\mathrm{r}} = 0$), the residual water level is usually small compared with the depth relative to mean sea level, i.e., $\overline{z} \ll \overline{h}$. However, it becomes important and affects tidal damping in the upstream part of an estuary where the influence of river discharge is considerable.

HESSD
11, 7053–7087, 2014

It should be noted that φ is a local parameter because it depends on the velocity amplitude υ which is a function of x (see Table 1). At the same time, the tidally averaged depth depends on the residual water level caused by the nonlinear friction term. Hence a fully explicit solution for the main dimensionless parameters (i.e., μ, δ, λ, ε) cannot be obtained. Therefore an iterative refinement is needed to obtain the correct wave behaviour. The following procedure usually converges in a few steps: (1) initially we assume $Q_f = 0$ and calculate the initial values for the velocity number μ, celerity number λ and the tidal velocity amplitude υ (and hence dimensionless river discharge term φ) explicitly using the analytical solution proposed by Cai et al. (2012); (2) taking into account the effect of river discharge Q_f, the revised damping number δ, velocity number μ, celerity number λ, velocity amplitude υ (and hence φ), and phase lag ε are calculated by solving Eqs. (T4), (T2), (T3) and (T1) using a simple Newton–Raphson method; (3) subsequently we account for the residual water level according to Eq. (15); (4) this process is repeated until the result is stable, after which the dimensional parameters (e.g., η, υ) are computed.

In order to follow along-channel variations of the estuarine sections, the iterative procedure is combined with a multi-reach approach (subdividing the whole estuary into short reaches), where the damping number δ is integrated in short reaches over which we assume the estuary shape number γ, the friction number χ, and the dimensionless river discharge term φ to be constant. This is done by using a simple explicit integration of the linear differential equation:

$$\eta_1 = \eta_0 + \frac{\mathrm{d}\eta}{\mathrm{d}x}\Delta x = \eta_0 + \frac{\delta\eta_0\omega\Delta x}{c_0}. \tag{18}$$

where η_0 is the tidal amplitude at the downstream end of every short reach, while η_1 the tidal amplitude at a distance Δx (e.g., 1 km) upstream.

HESSD
11, 7053–7087, 2014

3 Application to the Yangtze estuary

3.1 Geometry of the Yangtze estuary

The Yangtze River feeding the estuary is the largest river in China with an annual mean fresh water discharge of 28 300 $m^3 s^{-1}$ measured at the upstream boundary of the estuary at Datong station (1950–2010). The tide penetrates from the mouth (Zhongjun station) up to Datong at a distance of approximately 630 km (see Fig. 3). The tidal near the estuary mouth is mesotidal with a mean tidal range of 2.7 m with the dominant tidal constituent being semi-diurnal. The main geometic parameters (i.e., cross-sectional area, width and depth) along the estuary axis are shown in Fig. 4, along with best fitting lines based on Eq. (1). It can be seen that the whole estuary can be simplified as two reaches with the inflection point at $x = 275$ km (located between Jiangyin and Zhenjiang, see Fig. 3). The topographical parameters used to fit the geometry are presented in Table 3. We see that both the cross-sectional area and width exponentially decrease in landward direction from the estuary mouth, while there is a slight increase of the averaged depth in the seaward reach ($x = 0$–275 km). From 275 km upstream the depth gradually reduces. It is noted that the Yangtze estuary is a branched system, where the seaward part is divided by the Chongming Island into the North Branch and the South Branch. In this paper, we only focus on the South Branch and the upper reach, since the North Branch is much smaller compared to the South Branch, and functions in isolation (Zhang et al., 2012.).

3.2 Calibration and verification of the model

The analytical model presented in Sect. 2 was calibrated and verified with the monthly aveaged tidal amplitudes and water levels collected in 2005. Figure 5 shows the comparison between the measurments and the analytically computed tidal amplitude and tidally averaged depth along the estuary in 2005. We see that the correspondence with the observed values in each month is good, which suggests that the proposed

HESSD
11, 7053–7087, 2014

analytical model can well reproduce the tidal dynamics with a wide range of river discharge (11 600–48 000 $m^3 s^{-1}$). The calibrated Manning–Strickler friction coefficient K and storage width ratio r_S are presented in Table 4. A relatively larger K value in the seaward reach of 70 $m^{1/3} s^{-1}$ and 60 $m^{1/3} s^{-1}$ in the landward reach has been used to calibrate the model, which is reasonable since the downstream part has a higher mud content, distinguishing between riverine and marine dominated parts of the estuary. It is interesting to note that the calibrated r_S in the dry season (month 1, 2, 3, 4, 11 and 12) is larger than that in the wet season (month 5, 6, 7, 8, 9 and 10), which is possibly due to the fact that the influence of storage area (such as marshes and tidal flats) is much stronger in the dry season compared with that in the wet season. A possible explanation for this phenomenon is discussed below in Sect. 3.3. Figure 5 also shows the resulted residual water level due to nonlinear friction according to Eq. (15) (i.e., including bottom friction and river discharge). It can be seen that the residual water level is increased with river discharge, which indicates that the residual effect is more important in the wet season.

According to Eq. (2) the flow veloicty consists of two components: the tidal component with velocity amplitude υ and the velocity of the river discharge U_r. In Fig. 6 the two components and the ratio between them (i.e., φ defined in Table 1) are presented for the Yangtze estuary in 2005. A critical point can be defined where the river flow velocity is equal to the velocity amplitude (i.e., $\varphi = 1$), upstream of which the influence of river discharge is dominant over the tidal flow. We can see from Fig. 6 that the location of this point varies with river discharge. At a small discharge of 11 600 $m^3 s^{-1}$ in January, the velocity of the river discharge becomes dominant from 368 km onward, while with a large river discharge of 48 000 $m^3 s^{-1}$ in September this occurs at $x = 139$ km.

Figure 7 shows the variation of the wave celerity c and phase lag ε along the Yangtze estuary under different river discharge conditions. We see that the wave celerity c is smaller than the classical wave celerity c_0, which is mainly due to the fact that the Yangtze estuary is a damped estuary under significant influence of river discharge. As expected, we see that the classical wave celerity during the wet season is larger than

HESSD
11, 7053–7087, 2014

that during the dry season, due to the larger residual water level and smaller storage width ratio (according to Eq. 3). However, we see that the increase of the actual wave celerity is not significant, which is due to the counteraction of the tidal damping by river discharge (see the celerity Eq. T3 in Table 2). With regard to the variation of the phase lag, the values are in the range of 50–70°, which suggests that the tidal character is close to a progressive wave. Meanwhile, it can be seen that the bigger the river discharge the smaller the phase lag.

3.3 Effect of river discharge on tidal dynamics

With the analytical model presented in Sect. 2, the major mechanisms of how river discharge affects tidal dynamics can be identified. One mechanism is increasing friction, which can be seen from the damping Eq. (T4). The influence of river discharge on tidal dynamics is very similar to that of the friction number χ. This can be demonstrated by rewritting the friction parameter Γ_H in Eq. (6)

$$\Gamma_H = \begin{cases} \frac{2}{3}\mu\lambda\left[1+\frac{8}{3}\zeta\frac{\varphi}{\mu\lambda}+\left(\frac{\varphi}{\mu\lambda}\right)^2\right]+\frac{1}{3}\left(\frac{L_1}{2}-\zeta\frac{L_0}{3\mu\lambda}\right)= \\ \frac{2}{3}\mu\lambda\left[1+\frac{8}{3}\zeta\frac{\varphi}{\mu\lambda}+\left(\frac{\varphi}{\mu\lambda}\right)^2\right]+\frac{8}{9\pi}\left(\frac{3\pi}{16}L_1-\frac{\pi}{8}\frac{L_0\zeta}{\mu\lambda}\right) \qquad \text{for } \varphi<\mu\lambda \\ \frac{2}{3}\mu\lambda\left[\frac{4}{3}\zeta+2\frac{\varphi}{\mu\lambda}+\frac{4}{3}\zeta\left(\frac{\varphi}{\mu\lambda}\right)^2\right]+\frac{1}{3}\left(\frac{L_1}{2}-\zeta\frac{L_0}{3\mu\lambda}\right)= \\ \frac{2}{3}\mu\lambda\left[\frac{4}{3}\zeta+2\frac{\varphi}{\mu\lambda}+\frac{4}{3}\zeta\left(\frac{\varphi}{\mu\lambda}\right)^2\right]+\frac{8}{9\pi}\left(\frac{3\pi}{16}L_1-\frac{\pi}{8}\frac{L_0\zeta}{\mu\lambda}\right) \qquad \text{for } \varphi\geq\mu\lambda \end{cases}, \tag{19}$$

where we see that the influence of river discharge is basically that of increasing friction by a factor depending on the dimensionless river discharge φ (i.e., by comparing the last two terms in Eq. 19) with the right-hand side of Eq. (14).

HESSD
11, 7053–7087, 2014

The second mechanism is related to the residual water level caused by the nonlinear frictional effect according to Eq. (15), in which the river discharge plays an important role. We should recognize that this residual effect (indicating higher depth) partly acts the other way around, i.e., reducing the tidal damping, since it reduces the bottom friction (smaller χ) in Eq. (T4). Additionally, the residual water level induces a slight increase of the cross-sectional area convergence (a smaller γ), especially in the upstream part of the estuary with large depth divergence, since $1/a = 1/b - 1/|d|$, where the depth convergence length d is negative.

The third mechanism is linked to the storage area, which is represented by the storage width ratio r_S. As a result of the calibration in the Yangtze estuary (see Sect. 3.1), we note that the effect of the storage area on the tidal dynamics is stronger in the dry season (bigger r_S), which indicates more friction (larger χ) and lower channel convergence (smaller γ) compared with those in the wet season. This seasonal variation of the storage width ratio is illustrated in Fig. 8. In the case of low river discharge, the channel width changes more strongly than the depth, resulting in a dominant lateral flow between the storage area and the main channel over the tidal cycle. Conversely, the depth increases more substantially compared with the width in case of high river discharge, leading to a more dominant longitudinal flow in the storage area. As a result, the flow in the storage area is in the same direction as that in the main channel, which suggests a smaller storage width ratio for high river discharge condition.

To provide insights into the relative importance of these three mechanisms, we applied the analytical model under different river discharge conditions (varying between 5000 and 60 000 $m^3 s^{-1}$). A yearly averaged tidal amplitude of 1.36 m at Zhongjun station (2005) is imposed at the seaward boundary. The calibrated parameters (including the friction coefficient K and storage width ratio r_S) are fixed for the sensitivity experiments. For simplicity, we adopted the calibrated r_S in the dry season when the river discharge is below 25 000 $m^3 s^{-1}$, while using the r_S in the wet season for river discharge larger than 25 000 $m^3 s^{-1}$. In Fig. 9 we see that both the residual water level $\overline{z}$ and the parameter Γ_H are increased with river discharge, which counteract each other, leading

HESSD
11, 7053–7087, 2014

to changes in the friction term $\chi\mu\lambda\Gamma_H$ in the damping Eq. (T4), the friction number χ and the shape number γ. As the river discharge increases, we see from Fig. 9c that the friction number χ is decreased, which indicates a reduction of the bottom friction. However, it is noted that the whole friction term $\chi\mu\lambda\Gamma_H$ is increased with river discharge (see Fig. 9d), which suggests that the increased friction due to river discharge (Γ_H) is dominant over the reduced friction due to residual water level. On the other hand, the estuary shape number γ is decreased with river discharge for cases using the same r_S, which is due to an increase of the residual water level. The lower values of γ for small river discharge ($Q_f < 25\,000\,m^3\,s^{-1}$) in the seaward reach is mainly caused by the adoption of larger storage width ratio, since the depth divergence is rather small. Conversely, in the upstream reach, where the depth divergence is remarkable, we see a smaller γ for larger river discharge conditions.

The effect of river discharge on the main features of the tidal dynamics is shown in Fig. 10. We see that the tidal amplitude, velocity amplitude and phase lag are reduced with river discharge, especially in the upper reach of the estuary, where it gradually becomes more riverine in character (indicating larger river flow velocity, see Fig. 10c). The abrupt higher tidal amplitude observed near the estuary mouth (see Fig. 10a) for the cases of larger river discharge ($Q_f > 25\,000\,m^3\,s^{-1}$) is due to the assumption that the adopted storage width ratio is smaller in the wet season than in the dry season (see Table 2). With regard to the wave celerity, it tends to increase with river discharge although there is significant damping caused by river discharge. The reason is mainly due to the increase of residual water level when increasing the river discharge.

3.4 A new approach for estimating fresh water discharge

Reliable estimation of fresh water discharge into estuaries is a critical component of water resources management (e.g., salt intrusion, freshwater withdrawal, flood protection etc.), yet fresh water discharge into estuaries remains poorly observed, as it requires observations during a full tidal cycle. The analytical model for tidal wave propagation makes clear that tide and river discharge interact and are governed by the

HESSD
11, 7053–7087, 2014

damping Eq. (T4) in Table 2. As a result, it is possible to develop an analytical equation to determine river discharge based on measurements of tidal water levels. If the tidal damping δ and the tidally averaged depth (including residual water level) $\overline{h}$ are known, we are able to use the inverse analytical model to predict the fresh water discharge. Moftakhari et al. (2013) also proposed a method to predict the fresh water discharge based on analysis of tidal statistics, using known astronomical forcing. However, they did not recognize the importance of residual water level. As opposed to the regression model they used for fresh water discharge estimation, the method presented here is fully analytical and takes into account both the friction and residual water level.

Knowing δ and γ, the tidal variables ε, λ and μ can be determined using Eqs. (T1), (T3) and (T2). Subsequently the damping Eq. (T4) in the upstream river discharge-dominated zone ($\varphi \geq \mu\lambda$) is used to predict the fresh water discharge. Recalling that $L_0 = -2 - 4\varphi^2, L_1 = 4\varphi$ for the case of $\varphi \geq 1$ and rearranging Eq. (T4), it is possible to obtain a quadratic equation of φ:

$$\alpha_1\varphi^2 + \alpha_2\varphi + \alpha_3 = 0, \tag{20}$$

with

$$\alpha_1 = -4\chi_0\mu^2\zeta^2 / \left[3 - 16\zeta^2/3\right], \tag{21}$$

$$\alpha_2 = r_S\delta\mu\zeta/\lambda - 2\mu^3\chi_0\lambda\zeta / \left[1 - (4\zeta/3)^2\right] - (\mu\gamma - \delta\mu)\left(\sqrt{1+\zeta} - 1\right)/\lambda, \tag{22}$$

$$\alpha_3 = -\chi_0\mu^2\zeta^2\left(8\mu^2\lambda^2/9 + 2/9\right) / \left[1 - (4\zeta/3)^2\right] - \delta + \mu^2\gamma - \delta\mu^2, \tag{23}$$

where χ_0 is the reference friction number, defined as:

$$\chi_0 = \chi\left[1 - (4\zeta/3)^2\right]/\zeta = r_S g c_0 / \left(K^2\omega\overline{h}^{4/3}\right), \tag{24}$$

where the r_S and K are the calibrated parameters.

HESSD
11, 7053–7087, 2014

For given values of δ, γ, λ, μ, χ_0 and ζ, the positive solution is:

$$\varphi = \frac{-\alpha_2 - \sqrt{\alpha_2^2 - 4\alpha_1\alpha_3}}{2\alpha_1}. \quad (25)$$

With this solution for φ, an explicit solution can be obtained for Q_f:

$$Q_f = \overline{A}U_r = \overline{A}\varphi\upsilon. \quad (26)$$

As an example, Fig. 11 shows the estimates of the monthly averaged fresh water discharge Q_f between 2005 and 2009 at x = 456 km in the Yangtze estuary located between the two points where tidal observations can be obtained (i.e., Wuhu and Maanshan tidal stations, see Fig. 3). In this case we used the calibrated Manning–Strickler friction coefficient $K = 60\,m^{1/3}\,s^{-1}$ and the calibrated storage width ratio of $r_S = 1.5$. We see from Fig. 11 that the correspondence with observations is good ($R^2 = 0.86$), which suggests that the proposed analytical model can be a useful tool to have a first order estimation of fresh water discharge in the tidal region. The deviation from observations is probably related to the simplification of a rectangular cross-section and observational error.

Figure 12 shows the analytically predicted fresh water discharge for a range of tidally averaged depth $\overline{h}$ (9 to 20 m) and damping number δ (−2 to 0) according to Eq. (26). For simplicity, we assumed a fixed tidal amplitude at x = 456 km equal to the monthly averaged value of 0.14 m. It can be seen from Fig. 12 that the fresh water discharge is mainly determined by two controlling factors. Both the tidally averaged depth and the tidal damping tend to result in a larger fresh water discharge.

Further work will be required to test the accuracy of the explicit Eq. (26) with more detailed measurements (e.g., daily river discharge and water level).

HESSD
11, 7053–7087, 2014

4 Conclusions

An analytical model has been applied to the Yangtze estuary where the influence of river discharge is remarkable. The method involves solving a set of 4 implicit equations (i.e., the phase lag, the scaling, the celerity and the damping equations), in combination with an iterative procedure to account for the influence of residual water level due to nonlinear frictional effect. The results show a good agreement with observed tidal amplitude and water level in both dry and wet seasons, which suggest that the presented analytical model can be a powerful instrument for assessing the influence of human interventions (e.g., dredging, freshwater withdrawal) on tidal dynamics.

The effect of river discharge on tidal damping is not trivial, triggering different effects that partly counteract each other. We show that the river discharge affects tidal damping primarily through the friction term, and subsequently by the residual water level and the storage area, whereby the friction term and the storage area tend to increase the tidal damping, while the residual water level affects the tidal damping by reducing the bottom friction and increasing the cross-sectional area convergence length.

The relationship between water level (including residual water level) and river discharge, governed by the damping equation, enables us to develop a new method for estimating fresh water discharge in estuaries on the basis of tidal water level observations via an inverse analytical model. The limitation of such an approach is that it can only be applied in the upstream part of the estuary where the river discharge dominates over the tide.

Acknowledgements. The first author is financially supported for his Ph.D. research by the China Scholarship Council with the project reference number of 2010638037.

HESSD
11, 7053–7087, 2014

References

Cai, H., Savenije, H. H. G., and Toffolon, M.: A new analytical framework for assessing the effect of sea-level rise and dredging on tidal damping in estuaries, J. Geophys. Res., 117, C09023, doi:10.1029/2012JC008000, 2012. 7057, 7059, 7061

Cai, H., Savenije, H. H. G., and Toffolon, M.: Linking the river to the estuary: influence of river discharge on tidal damping, Hydrol. Earth Syst. Sci., 18, 287–304, doi:10.5194/hess-18-287-2014, 2014. 7055, 7057, 7058, 7060, 7073

Dronkers, J. J.: Tidal Computations in River and Coastal Waters, Elsevier, New York, 1964. 7058

Hidayat, H., Hoitink, A., Sassi, M., and Torfs, P.: Prediction of discharge in a tidal river using artificial neural networks, J. Hydrol. Eng., doi:10.1061/(ASCE)HE.1943-5584.0000970, online first, 2014. 7055

Miller, W. D., Kimmel, D. G., and Harding, L. W.: Predicting spring discharge of the Susquehanna River from a winter synoptic climatology for the eastern United States, Water Resour. Res., 42, W05414, doi:10.1029/2005WR004270, 2006. 7055

Moftakhari, H. R., Jay, D. A., Talke, S. A., Kukulka, T., and Bromirski, P. D.: A novel approach to flow estimation in tidal rivers, Water Resour. Res., 49, 4817–4832, doi:10.1002/wrcr.20363, 2013. 7055, 7067

Negrel, J., Kosuth, P., and Bercher, N.: Estimating river discharge from earth observation measurements of river surface hydraulic variables, Hydrol. Earth Syst. Sci., 15, 2049–2058, doi:10.5194/hess-15-2049-2011, 2011. 7055

Savenije, H. H. G.: Analytical expression for tidal damping in alluvial estuaries, J. Hydraul. Eng.-ASCE, 124, 615–618, doi:10.1061/(ASCE)0733-9429(1998)124:6(615), 1998. 7057

Savenije, H. H. G.: Salinity and Tides in Alluvial Estuaries, Elsevier, New York, 2005. 7056, 7060

Savenije, H. H. G.: Salinity and Tides in Alluvial Estuaries, completely revised 2nd edn., available at: www.salinityandtides.com (last access: 20 May 2014), 2012. 7054, 7056

Savenije, H. H. G., Toffolon, M., Haas, J., and Veling, E. J. M.: Analytical description of tidal dynamics in convergent estuaries, J. Geophys. Res., 113, C10025, doi:10.1029/2007JC004408, 2008. 7055, 7056, 7057

Toffolon, M. and Savenije, H. H. G.: Revisiting linearized one-dimensional tidal propagation, J. Geophys. Res., 116, C07007, doi:10.1029/2010JC006616, 2011. 7057

HESSD
11, 7053–7087, 2014

Toffolon, M., Vignoli, G., and Tubino, M.: Relevant parameters and finite amplitude effects in estuarine hydrodynamics, J. Geophys. Res., 111, C10014, doi:10.1029/2005JC003104, 2006. 7057

Vignoli, G., Toffolon, M., and Tubino, M.: Non-linear frictional residual effects on tide propagation, in: Proceedings of XXX IAHR Congress, vol. A, Thessaloniki, Greece, 24–29 August 2003, 291–298, 2003. 7060

Zhang, E. F., Savenije, H. H. G., Chen, S. L., and Chen, J. Y.: Water abstraction along the lower Yangtze River, China, and its impact on water discharge into the estuary, Phys. Chem. Earth, 47–48, 76–85, doi:10.1016/j.bbr.2011.03.031, 2012a. 7055

Zhang, E. F., Savenije, H. H. G., Chen, S. L., and Mao, X. H.: An analytical solution for tidal propagation in the Yangtze Estuary, China, Hydrol. Earth Syst. Sci., 16, 3327–3339, doi:10.5194/hess-16-3327-2012, 2012b. 7055, 7062

HESSD

11, 7053–7087, 2014

Table 1. Definition of dimensionless parameters.

Dimensionless parameters	
Local variable	Dependent variable
Tidal amplitude $\zeta = \eta/\overline{h}$	Damping number $\delta = c_0 \mathrm{d}\eta/(\eta\omega \mathrm{d}x)$
Estuary shape $\gamma = c_0/(\omega a)$	Velocity number $\mu = \upsilon/(r_S \zeta c_0) = \upsilon\overline{h}/(r_S \eta c_0)$
Friction number $\chi = r_S f c_0 \zeta/(\omega\overline{h})$	Celerity number $\lambda = c_0/c$
River discharge $\varphi = U_r/\upsilon$	Phase lag $\varepsilon = \pi/2 - (\phi_Z - \phi_U)$

HESSD
11, 7053–7087, 2014

Table 2. Analytical solutions for tidal dynamics accounting for river discharge (Cai et al., 2014).

Cases	Phase lag $\tan(\varepsilon)$	Scaling μ	Celerity λ^2	Damping δ
General	$\lambda/(\gamma-\delta)$ (T1)	$\sin(\varepsilon)/\lambda = \cos(\varepsilon)/(\gamma-\delta)$ (T2)	$1-\delta(\gamma-\delta)$ (T3)	$\mu^2(\gamma\theta - \chi\mu\lambda\Gamma_H)/(1+\mu^2\beta)$ (T4)
Ideal estuary	$1/\gamma$	$\sqrt{1/(1+\gamma^2)}$	1	0

HESSD
11, 7053–7087, 2014

Table 3. Geometric characteristics in the Yangtze estuary.

Reach (km)	Depth $\overline{h}$ (m)	Convergence length a (km)	Convergence length b (km)	Convergence length d (km)
0–275	10.4	143	127	−1135
275–580	9.2	432	1349	636

HESSD
11, 7053–7087, 2014

Table 4. Calibrated parameters used in the analytical model.

Reach (km)	Manning–Strickler friction K ($m^{1/3} s^{-1}$)	Storage width ratio r_S	
		Dry season (1, 2, 3, 4, 11, 12)	Wet season (5, 6, 7, 8, 9, 10)
0–275	70	1.4	1
275–580	60	1.8	1

HESSD
11, 7053–7087, 2014

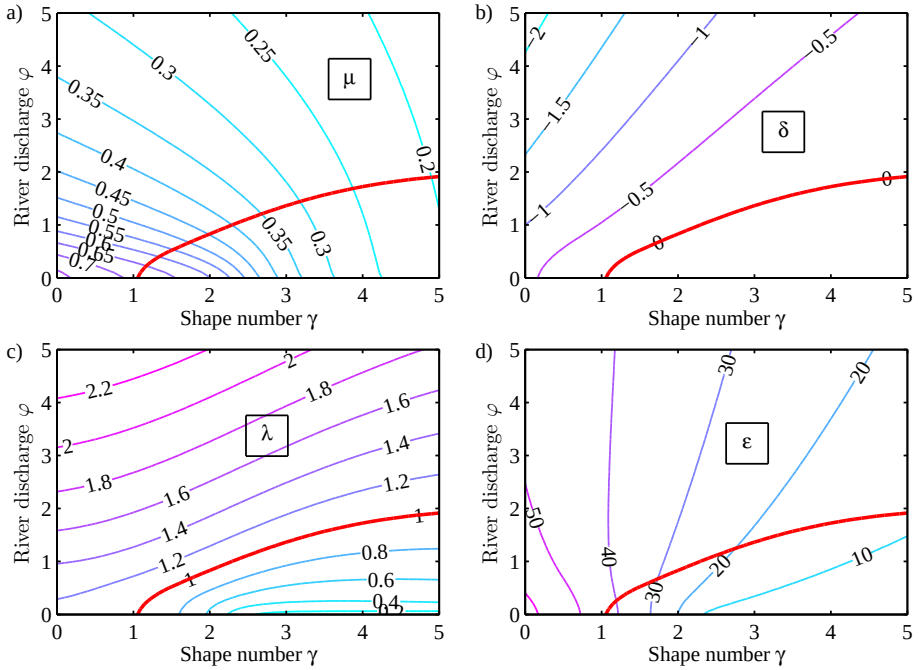

Figure 1. Contour plot of the main dependent parameters – **(a)** μ, **(b)** δ, **(c)** λ, **(d)** ε – as a function of the estuary shape number γ and the dimensionless river discharge term φ obtained by solving Eqs. (T1)–(T4) (see Table 2) for given $\zeta = 0.1$, $\chi = 2$ and $r_S = 1$. The thick red lines represent the ideal estuary, where $\delta = 0$ and $\lambda = 1$.

HESSD
11, 7053–7087, 2014

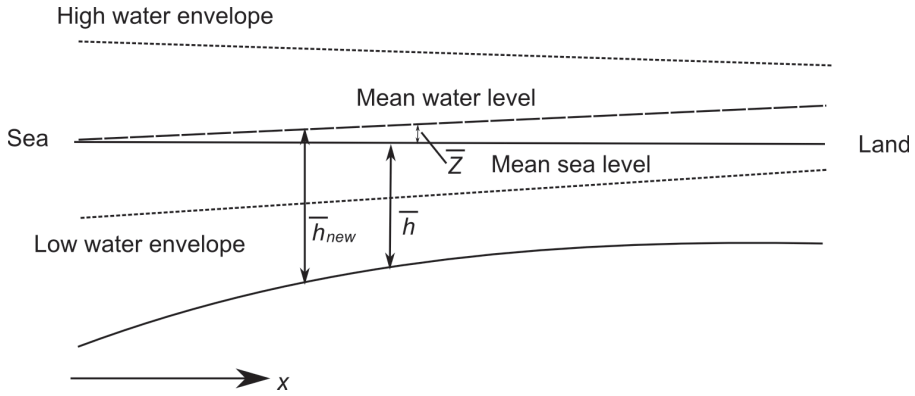

Figure 2. Sketch of the water levels in an estuary, where $\overline{z}$ is the residual water level.

HESSD
11, 7053–7087, 2014

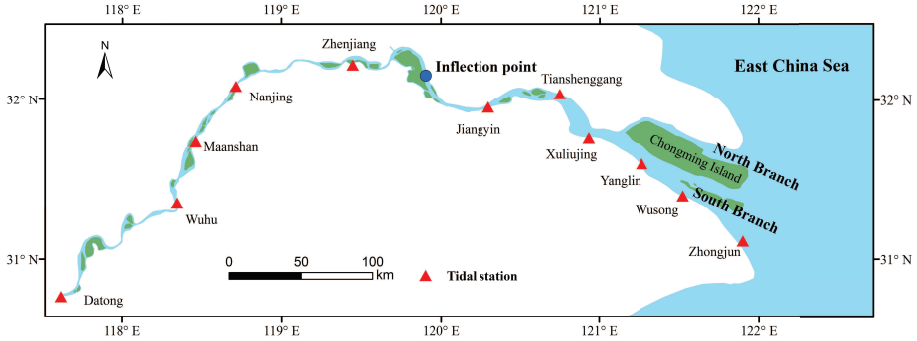

Figure 3. Sketch of the Yangtze estuary in China.

HESSD
11, 7053–7087, 2014

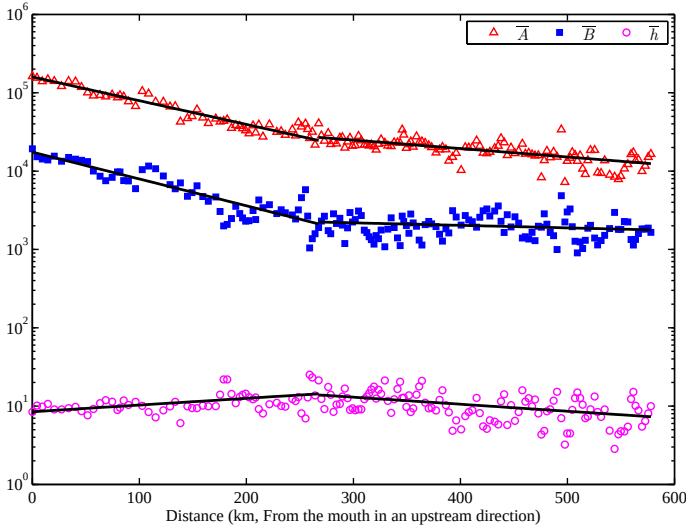

Figure 4. Semi-logarithmic plot of the tidally averaged cross-sectional area $\overline{A}$ (triangles), width $\overline{B}$ (squares), and depth $\overline{h}$ (circles) in the Yangtze estuary. The drawn lines represent the fitted exponential curves.

HESSD
11, 7053–7087, 2014

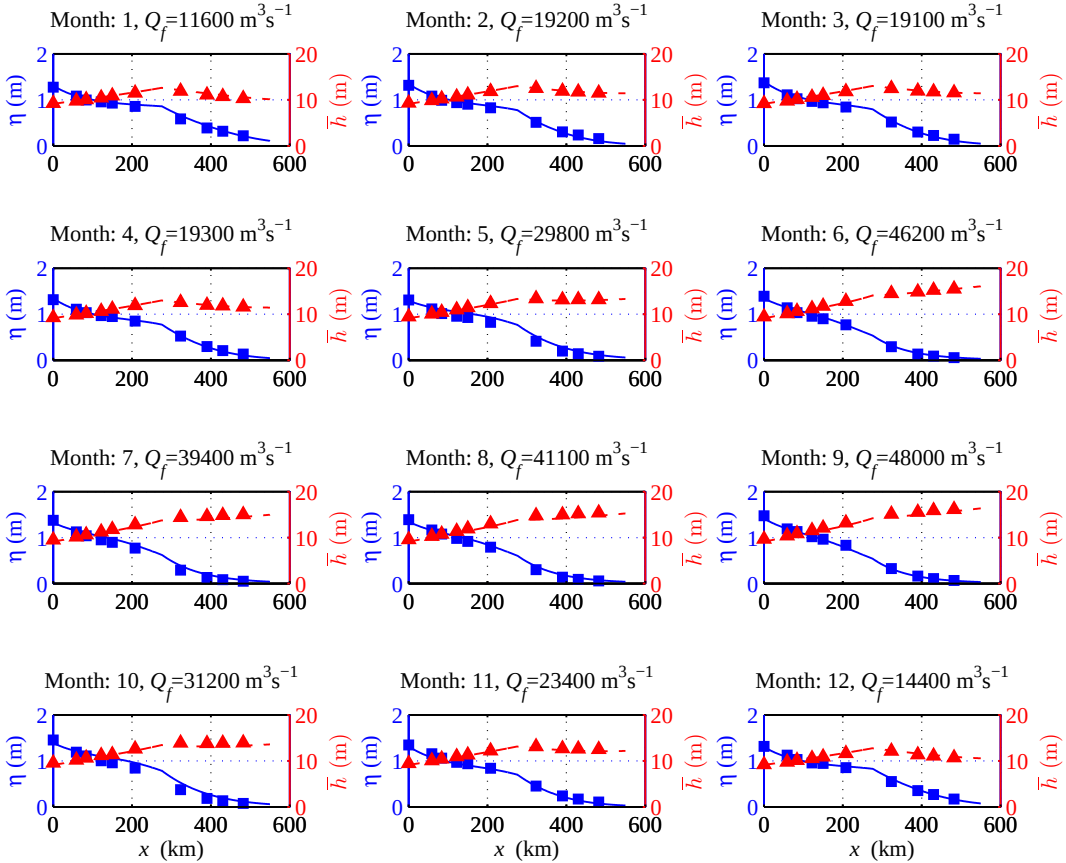

Figure 5. Comparison between analytically computed monthly-averaged values (left-hand vertical scale: tidal amplitude; right-hand vertical scale: depth including the residual water level) and observations in the Yangtze estuary in 2005.

HESSD
11, 7053–7087, 2014

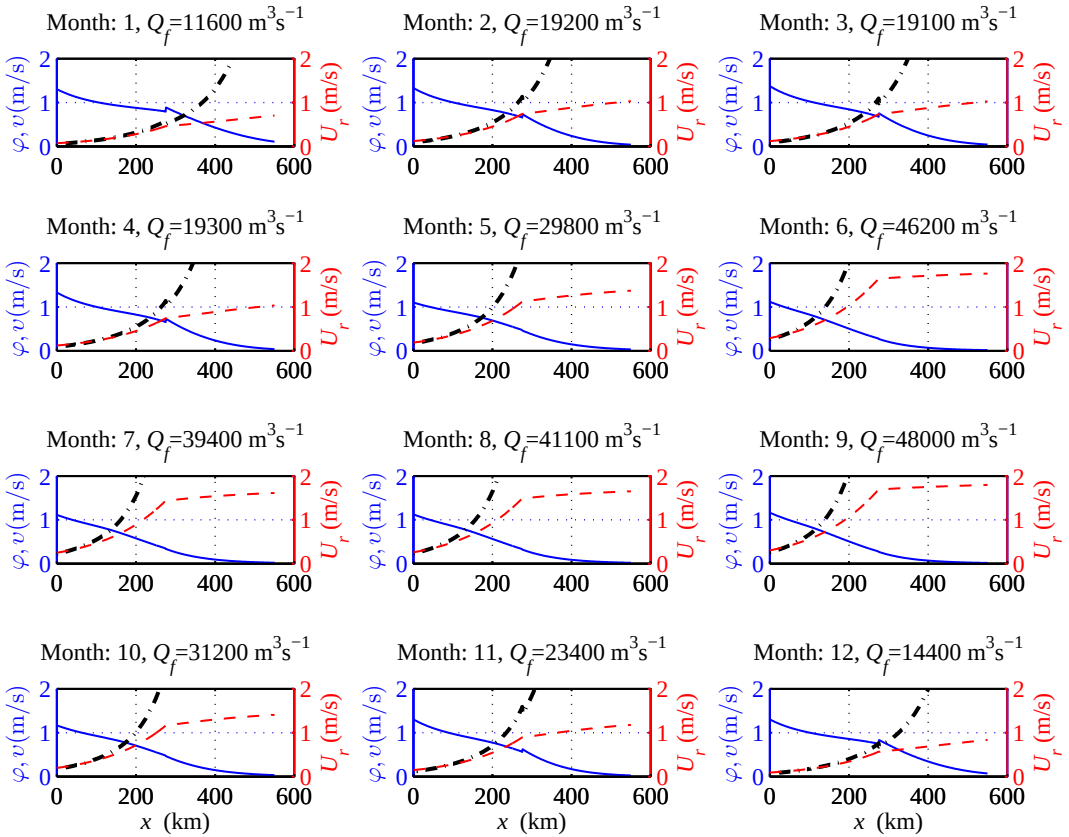

Figure 6. Longitudinal variation of the tidal velocity amplitude υ and river flow velocity U_r along the Yangtze estuary in 2005. The dashed-dotted line represents the ratio of the river flow velocity to the tidal veloicty amplitude (i.e., the dimensionless river discharge term φ).

HESSD
11, 7053–7087, 2014

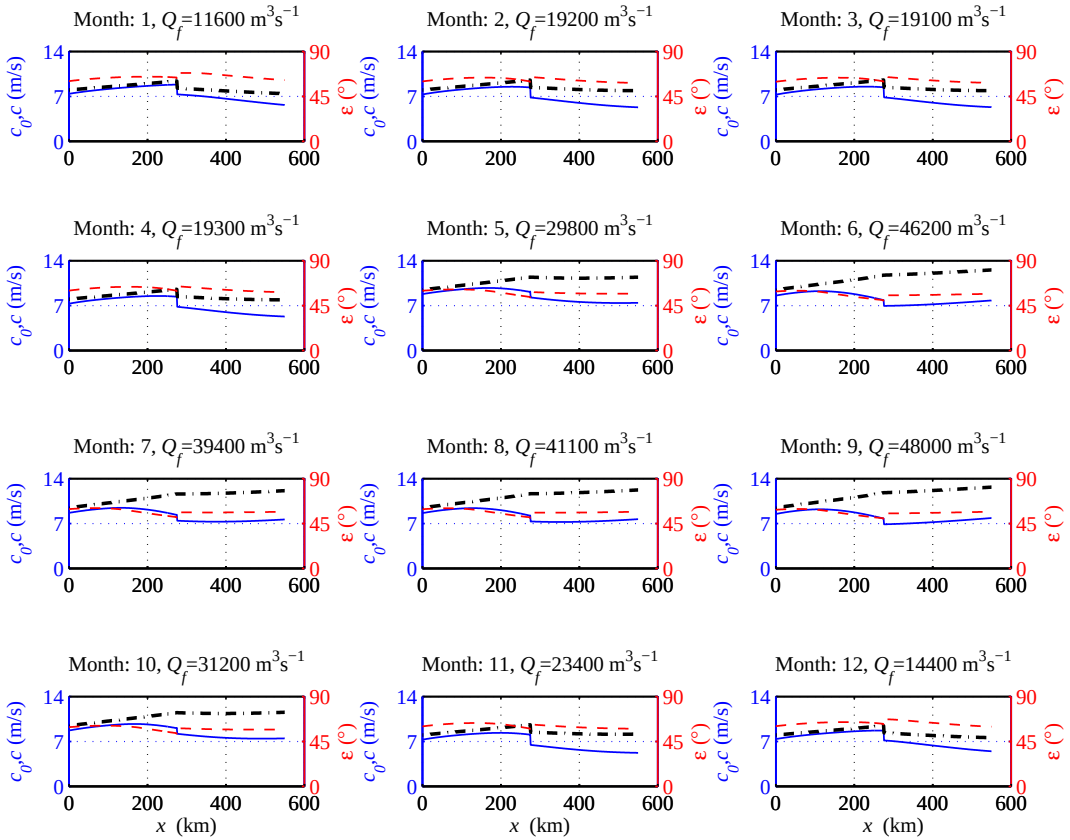

Figure 7. Longitudinal variation of the wave celerity c (blue) and the phase lag ε (red) along the Yangtze estuary in 2005. The dashed-dotted line represents the classical wave celerity c_0 from Eq. (3).

HESSD
11, 7053–7087, 2014

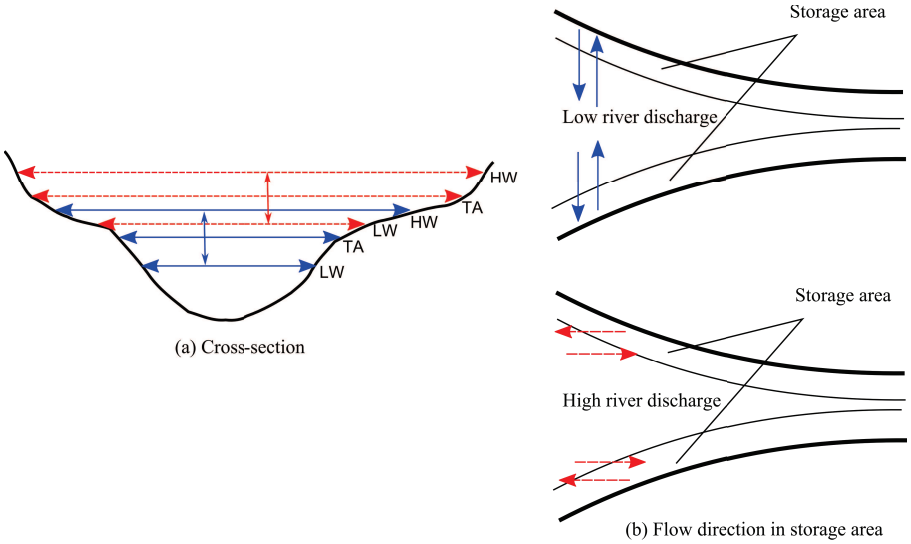

Figure 8. Variation of the water levels (LW: low water level, TA: tidally averaged water level, HW: high water level) in a cross-section **(a)** and the dominated flow direction in the storage area **(b)**. The blue drawn line represents the case with low river discharge, while the red dashed line represents the case with high river discharge.

HESSD
11, 7053–7087, 2014

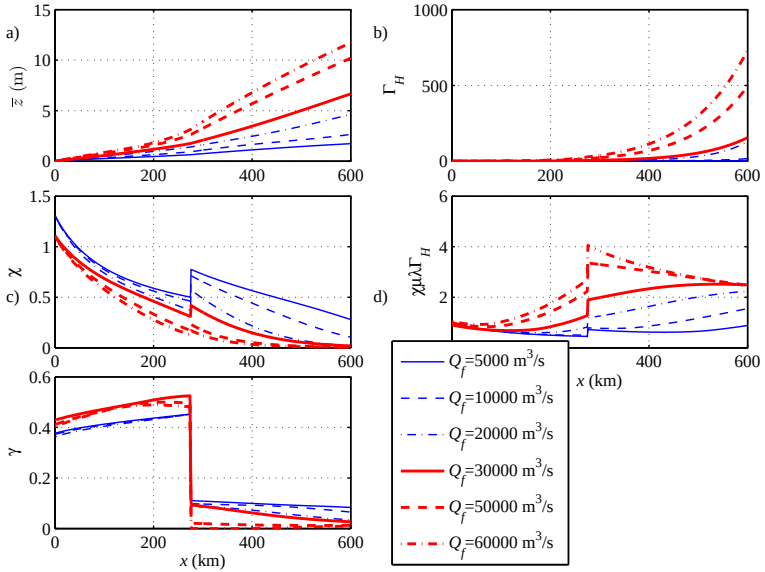

Figure 9. Longitudinal variation of the residual water level $\bar{z}$ **(a)**, the parameter Γ_H **(b)**, the friction number χ **(c)**, the friction term $\chi\mu\lambda\Gamma_H$ in (T4), and the shape number γ **(e)** in the Yangtze estuary under different river discharge conditions.

HESSD
11, 7053–7087, 2014

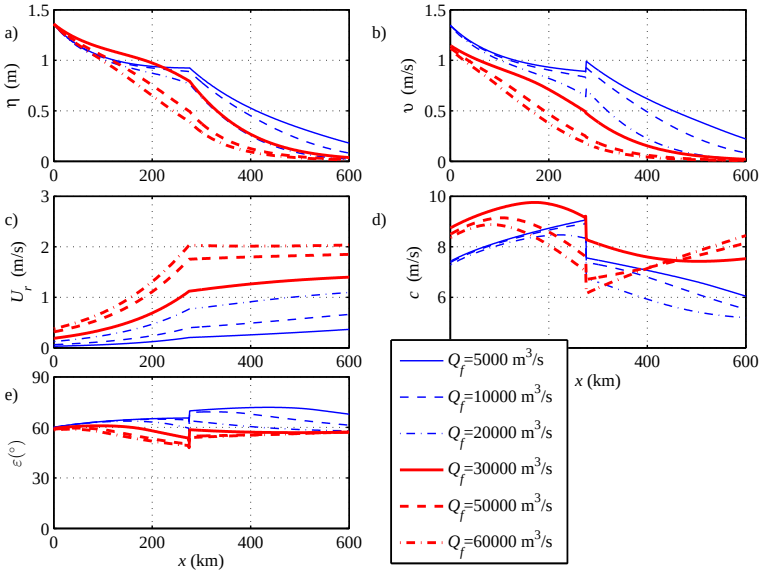

Figure 10. Longitudinal variation of the tidal amplitude η **(a)**, the velocity amplitude υ **(b)**, the river flow velocity U_r **(c)**, the wave celerity c **(d)**, and the phase lag ε **(e)** in the Yangtze estuary under different river discharge conditions.

HESSD
11, 7053–7087, 2014

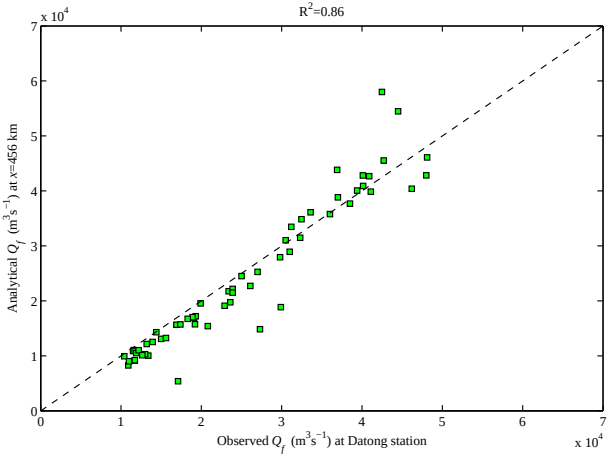

Figure 11. Comparison between analytically predicted fresh water discharge and observations (at Datong tidal station) in the Yangtze estuary in different months during 2005–2009. R^2 is the coefficient of determination.

HESSD
11, 7053–7087, 2014

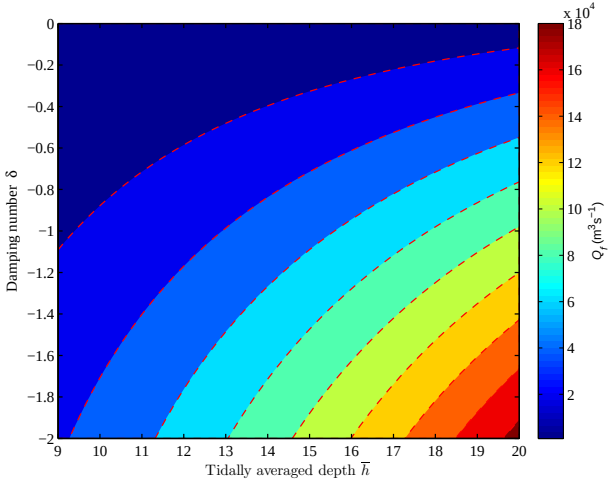

Figure 12. Contour plot of the predicted fresh water discharge at $x = 456$ km as a function of the tidally averaged depth $\overline{h}$ and the damping number δ for given tidal amplitude $\eta = 0.14$ m, convergence length $a = 432$ km, Manning–Strickler friction coefficient $K = 60\,\mathrm{m}^{1/3}\,\mathrm{s}^{-1}$, and storage width ratio $r_S = 1.5$.

HESSD
11, 7053–7087, 2014